ELSEVIER

Earth and Planetary Science Letters 123 (1994) 205–220

EPSL

Ferric iron in peridotites and mantle oxidation states

D. Canil [a,1], H.St.C. O'Neill [a], D.G. Pearson [b], R.L. Rudnick [c], W.F. McDonough [c], D.A. Carswell [d]

[a] *Bayerisches Geoinstitut, Universität Bayreuth, Postfach 101251, D-95440 Bayreuth, Germany*
[b] *Department of Earth Sciences, Open University, Milton Keynes, MK7 6AA, UK*
[c] *Research School of Earth Sciences, Australian National University, Canberra ACT 2601, Australia*
[d] *Department of Earth Sciences, University of Sheffield, Sheffield S3 7HF, UK*

(Received October 29, 1993; revision accepted March 10, 1994)

Abstract

^{57}Fe Mössbauer spectroscopy is employed to estimate $Fe^{3+}/\Sigma Fe$ ratios and the Fe_2O_3 content of 28 well characterized pyroxenite and peridotite xenoliths from central France, southeastern Australia, northern Tanzania, southern Africa and Siberia. The Fe_2O_3 contents of various mantle regions were assessed, and found to range from 0.1 to 0.4 wt%. With an appraisal of the likely mantle inventories of C, H and S, the results demonstrate that these volatile elements and Fe all have similar buffering capacities for oxygen in peridotites. For this reason, the oxidation states of upper mantle peridotites should not generally be controlled by any particular buffer system.

New estimates for the oxidation states of cratonic garnet peridotites indicate that the upper mantle beneath cratons is within 1 log unit of the fayalite–magnetite–quartz (FMQ) buffer, but may have been progressively oxidized since its original formation in the early Archean.

1. Introduction

The oxygen fugacity (fO_2) of the Earth's mantle plays an important role during magma generation and is a major constraint on degassing models for the formation of the hydrosphere and atmosphere [1]. The fO_2 in the spinel lherzolite facies of the upper mantle varies nearly six orders of magnitude, from 2 log units above to 4 log units below the FMQ buffer (FMQ + 2 to FMQ − 4), depending on the tectonic provenance of the particular samples studied [2,3]. Preliminary estimates based on the Fe^{3+} content of garnets from peridotite xenoliths suggest fO_2 values for the garnet lherzolite facies similar to those for spinel lherzolite xenoliths [4] and kimberlite-hosted ilmenites [5,6]. In contrast, mineral assemblages in diamonds may record consistently lower fO_2, between FMQ − 3 and FMQ − 4 [1].

Although much is currently known about the oxidation states of mantle-derived samples, questions remain as to what controls fO_2 in the mantle. For example, Fe^{3+}/Fe^{2+} equilibria amongst silicates and oxides may buffer oxygen fugacities and fluid speciation between C, H and S, the most important volatiles in the mantle. Conver-

[UC]

[1] Present Address: School of Earth and Ocean Sciences, University of Victoria, P.O. Box 1700 Victoria, B.C. V8W 2Y2, Canada.

SSDI 0012-821X(94)00052-Z

sely, equilibria between these volatile elements may control Fe^{3+}/Fe^{2+} equilibria in mantle silicates and oxides by reactions of the type:

$$2\ \underset{\text{silicate}}{FeO} + CO_2 = = \underset{\text{silicate}}{Fe_2O_3} + C \quad (1)$$

$$2\ \underset{\text{silicate}}{FeO} + H_2O = = \underset{\text{silicate}}{Fe_2O_3} + H_2 \quad (2)$$

$$2\ \underset{\text{silicate}}{FeO} + SO_2 = = \underset{\text{silicate}}{Fe_2O_3} + S_2 \quad (3)$$

which, if any buffer equilibria actually controls mantle oxidation states, will be governed by the abundance of the element with variable valence state, the moles of oxygen exchanged (or 'buffering capacity') in the respective redox equilibrium and the fluid species stable along a given geotherm.

The purpose of this study is to derive an accurate estimate for the abundance of Fe_2O_3 in various mantle samples and to investigate in detail the geochemistry of ferric iron in upper mantle processes. These data permit a more accurate comparison of the buffering capacity of Fe in the upper mantle, relative to the volatile elements C, H and S, and help elucidate the factors controlling mantle oxidation states. New estimates for the oxygen fugacities of garnet lherzolites from cratonic mantle lithosphere are presented and are used to examine secular or spatial variation in the oxidation states of the subcontinental mantle lithosphere.

2. Samples and approach

Estimates of the Fe^{3+} content of upper mantle peridotites in this study are made by determining the Fe^{3+} content of each individual phase by ^{57}Fe Mössbauer spectroscopy and multiplying by its modal abundance and total Fe, as determined by electron microprobe analysis. This approach is possible only for reasonably large samples ($\sim$ 500 g) with both bulk and mineral chemical data, from which modes can be calculated from the mineral chemical data by least-squares mass balance, and for which sufficient clean mineral separates of each phase are available.

The samples studied are pyroxenites and peridotites from a variety of locations, representing a broad range in tectonic settings, mineralogy and major element geochemistry (Table 1). Petrographic, isotopic, mineral and geochemical data for most of these samples appear in more extended studies (Table 1) and will not be elaborated upon here. The analytical procedures are given in the Appendix.

A more conventional method for determining the $Fe^{3+}/\Sigma Fe$ of mantle minerals or bulk rocks is by wet chemical methods. However, wet chemical analysis for $Fe^{3+}/\Sigma Fe$ in both minerals and whole

Table 1
Sample descriptions

Sample	Rock Type[a]/Description[b]	Locality	Age[c] (Ma)	Reference
Southeastern Australia			< 3	[7]
84-402	sp lherz, equigranular	Porndon		
85-168[e]	sp lherz, granuloblastic tabular	Leura		
84-413[e]	phl wehr, secondary recrystallized	Noorat		
84-438[e]	phl wehr, porphyroclastic	Shadwell		
BM134[e]	amp-sp lherz, porphyroclastic	Bullenmeri		
2905	sp lherz, protogranular tabular	Noorat		
Tanzania			< 3	[8,9]
89-661[e]	gt lherz, coarse	Lashaine		
89-669	wehr, protogranular	Lashaine		
89-772[e]	dun, protogranular	Olmani		
89-680	gt harz, coarse	Lashaine		
89-719	gt harz, coarse	Lashaine		
89-777[e]	wehr, protogranular	Olmani		
89-773[e]	harz, protogranular	Olmani		
Southern Africa				
BD1140[e]	gt lherz, coarse, low T	Bultfontein	83±3	[10]
BD1150[e]	gt lherz, coarse, low T	Bultfontein		[10]
BD1201	gt lherz, coarse, low T	Wesselton	88±2	[10]
BD1354	gt webs, coarse, low T	Matsoku		[10]
PHN5273	gt harz, coarse, low T	Premier	1179±39	
FRB1350	sp-gt lherz+C, coarse, low T	Premier		[11]
FRB921	gt webs, coarse, low T	Premier		
FRB909	gt lherz, sheared, high T	Premier		
PHN5239	gt lherz, sheared, high T	Premier		
PHN5267	gt lherz, sheared, high T	Premier		[4,12]
F865	gt harz+C, coarse, low T	Finsch	119±3	[13]
F556	gt harz+C, coarse, low T	Finsch		[13,14]
Siberia				
UV417/89	gt lherz, coarse, low T	Udachnaya	350	
UV61/91	gt lherz, sheared, high T	Udachnaya		
Massif Central				
Fr1	sp lherz	Landoz	< 5	[15]

[a] Lherz = lherzolite; harz = harzburgite; dun = dunite; wehr = wehrlite; webs = websterite; sp = spinel; gt = garnet; phl = phlogopite; amp = amphibole; C = graphite or diamond. [b] Texture classification according to Harte [16] for spinel-bearing assemblages and Boyd and Mertzman [17] for garnet-bearing assemblages. [c] Emplacement age of host magma. Ages for southern African kimberlites from Allsopp et al. [18]. Age for Udachnaya from N. Pokhilenko (pers. commun.). [d] Olivine measured by ^{57}Mössbauer spectroscopy, no Fe^{3+} detected.

rock samples from this study almost invariably gives inflated values (Figs. 1 and 2) which are inconsistent with mass balance considerations for Fe amongst the phases in peridotites [25]. The inflated $Fe^{3+}/\Sigma Fe$ ratios produced by wet chemical analysis may be due to the oxidation of samples during acid digestion, or to the presence of oxidized interstitial material along the grain boundaries of bulk rock specimens.

3. Abundance and distribution of ferric iron

Studies of a modally metasomatized xenolith report that mantle olivines can contain $Fe^{3+}/\Sigma Fe$ up to 0.06 [26,27], implying that this phase alone would dominate the inventory of Fe^{3+} in peridotite. However, the olivine with a $Fe^{3+}/\Sigma Fe$ of 0.05 analyzed by McGuire et al. [26] contains laihunite, a well known, thermodynamically metastable, low-temperature alteration mineral and host for Fe^{3+}. Given the petrographic observations reported for this olivine [26,27], it is evident that the Fe^{3+} considered to be in olivine is, instead, hosted in inclusions or lamellae of laihunite and/or iron oxide phases and, therefore, cannot, sensu stricto, be considered as Fe^{3+} in the mantle olivine structure.

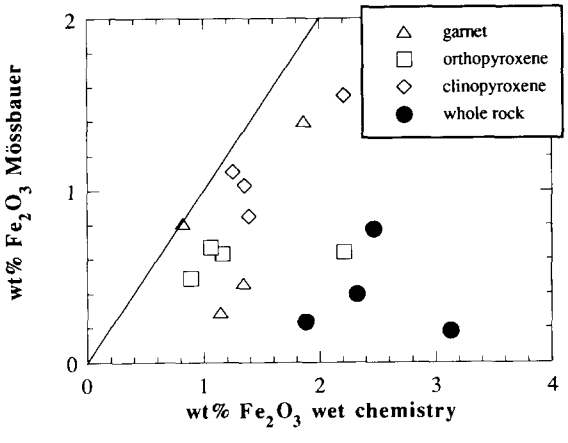

Fig. 1. Comparison of Fe_2O_3 contents for bulk rocks and minerals determined by ^{57}Mössbauer spectroscopy and wet chemical methods for garnet peridotites BD1140, BD1150, BD1201 and BD1354 in Table 1. Wet chemical data from [10]. Diagonal line represents 1:1 correlation.

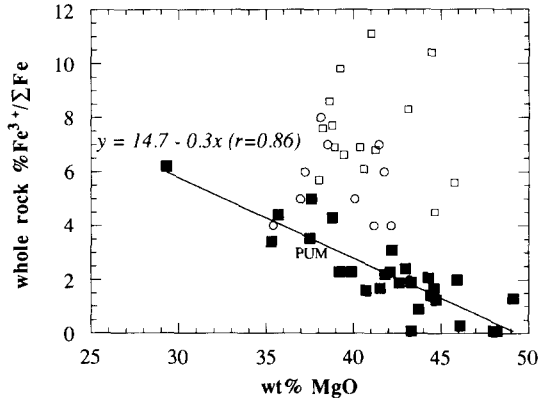

Fig. 2. Bulk MgO versus percentage $Fe^{3+}/\Sigma Fe$ ratio for samples from this study (solid squares) compared to those determined by wet chemical methods by Stolz and Davies [23] and Press et al. [24] (open squares and circles, respectively). Note the inflated values of $Fe^{3+}/\Sigma Fe$ at a given MgO content for samples measured by wet chemistry relative to the Mössbauer-derived estimates. The regression line for samples in this study (squares) results in a $Fe^{3+}/\Sigma Fe$ of 3.5% for primitive upper mantle (PUM), with 37 ± 1 wt% MgO [15,29], identical to that determined for the fertile peridotite Fr1 studied by Jagoutz et al. [15] (Table 2, Fig. 3). Samples with $Fe^{3+}/\Sigma Fe$ of 2.9–0.9%, containing greater than 37 wt% MgO (i.e. mantle residues) can be explained by 5–40% batch melting of primitive upper mantle, assuming a constant $D^{Fe_2O_3} = 0.1$.

There are stringent crystal chemical limits on the amount of Fe^{3+} that can be accommodated in Mg-rich mantle olivine [25], as demonstrated by experiment [28]. Nonetheless, to investigate the possibility of significant Fe^{3+} in mantle olivine further, both clean and visibly altered olivines (especially chosen to have red discoloration), olivines from xenoliths containing a hydrous phase and olivines from serpentinized xenoliths, were analyzed from nine samples in this study. All of these samples were found to contain $Fe^{3+}/\Sigma Fe$ below the detection level of the ^{57}Fe Mössbauer technique ($Fe^{3+}/\Sigma Fe \leqslant 0.01$ [22]). The search for significant Fe^{3+} in olivines from the remainder of the samples in Table 1 was eventually abandoned.

In orthopyroxene, $Fe^{3+}/\Sigma Fe$ varies between 0.05 and 0.10 (Table 2). At $Fe^{3+}/\Sigma Fe$ levels of 0.05, the contribution of Fe^{3+} to the ^{57}Fe Mössbauer spectra for orthopyroxene is difficult to resolve. Fits with $Fe^{3+}/\Sigma Fe$ ratios between 0.02 and 0.05 could sometimes be achieved with equal

Table 2
Modal and bulk compositions

Sample	84-402	85-168	84-413	84-438	BM134	2905	89-661	89-669	89-772
Mode									
Ol	66	69	49	72	79	60	87	86	97
Opx	29	24	19	–	12	24	6.1	0.9	
Cpx	2.9	4.2	12.8	19.1	3	13.3	4.2	8.6	3.4
Sp	1.4	0.5	–	0.22	0.1	2.2	0.5		
Gt	–	–	–	–	–	–	–	–	–
Phl	–	–	16.6	9.9	–	–	–	–	–
Amp	–	–	–	–	6.6	–	–	–	–
$Fe^{3+}/\Sigma Fe$									
Ol	–	–	nd	nd	nd	nd	–	–	–
Opx	0.06	0.06	0.07 *	–	0.05	0.06	0.08	0.07	–
Cpx	0.18	0.19	0.16	0.19	0.16	0.16	0.31	0.27 *	0.27
Sp	0.19	0.22	–	–	–	0.15	0.28	–	–
Gt	–	–	–	–	–	–	–	–	–
Phl	–	–	0.36	0.76	–	–	–	–	–
Amp	–	–	–	–	0.31	–	–	–	–
WR	0.019	0.017	0.034	0.043	0.013	0.022	0.009	0.008	0.003
SiO_2	44.1	44.0	44.1	42.4	43.1	45.1	42.4	40.8	40.6
MgO	44.5	42.4	36.1	39.8	44.4	39.8	48.1	43.7	46.1
Fe_2O_3	0.17	0.20	0.41	0.42	0.13	0.19	0.07	0.09 *	0.039
ΣFeO	7.8	9.8	8.5	8.5	8.8	7.6	6.8	9.5	12.5
CaO	0.87	1.20	2.6	3.71	1.22	2.84	0.94	1.75	0.66
Al_2O_3	1.27	1.66	2.9	2.44	1.25	3.13	0.7	0.55	0.11
TiO_2	0.05	0.12	0.83	0.32	0.04	0.11	0.08	0.1	0.02
Na_2O	0.07	0.10	0.39	0.44	0.32	0.24	0.12	0.2	0.05
Cr_2O_3	0.46	0.47	0.38	0.35	0.35	0.44	0.34	0.34	0.14
Total	99.1	99.8	95.8	97.3	99.5	99.3	99.5	97.0	100.2

Sample	89-680	89-719	89-777	89-773	BD1140	BD1150	BD1201	BD1354	PHN5273
Mode									
Ol	73	83	92	82	66	49	60	26.5	56
Opx	20	11.5	tr	17.5	17.3	24.6	29.5	35.9	37.1
Cpx	2.8	1.2	6.9	–	5.9	13.7	5.0	15.8	4.6
Sp	0.7	–	1.2	0.9	–	–	–	–	–
Gt	3.2	4.5	–	–	10.5	12.2	5.3	21.0	2.5
$Fe^{3+}/\Sigma Fe$									
Ol	–	–	–	–	nd	nd	–	–	–
Opx	0.09	0.09	–	0.06	0.09	0.10	0.10	0.06	–
Cpx	0.36	0.29	0.21	–	0.33	0.32	0.41	0.26	–
Sp	0.28	–	0.26	0.29	–	–	–	–	–
Gt	–	0.048	–	–	0.051	0.083	0.033	0.098	0.119
WR	0.019	0.009	0.007	0.014	0.022	0.049	0.030	0.062	–
SiO_2	44.3	43.4	41.3	44.0	45.0	46.8	46.8	47.9	47.4
MgO	45.9	47.7	48.2	49.1	41.8	37.6	42.2	29.3	43.2
Fe_2O_3	0.14	0.07	0.07	0.09	0.18	0.39	0.23	0.77	–
ΣFeO	6.6	6.8	8.5	5.97	7.3	7.1	6.8	11.2	6.5
CaO	0.81	0.55	1.36	0.11	1.75	3.49	1.33	4.38	1.11
Al_2O_3	1.22	1.09	0.17	0.39	2.58	3.05	1.52	4.85	1.15
TiO_2	0.03	0.02	0.05	0.01	0.17	0.11	0.07	0.2	0.15
Na_2O	0.05	0.13	0.07	0.02	0.21	0.4	0.12	0.44	0.08
Cr_2O_3	0.44	0.27	0.35	0.36	0.34	0.52	0.34	0.85	0.32
Total	99.5	100.0	100.0	100.0	99.2	99.1	99.2	99.1	99.9

Table 2 (continued)

Sample	FRB1350	FRB921	FRB909	PHN5239	PHN5267	F865	F556	UV417/89	UV61/91	Fr1
Mode										
Ol	55	27.5	58	67	63	66	47	54	70	52
Opx	32.8	42.3	32.2	26.1	20.2	27.6	46.1	18.6	19.4	28.1
Cpx	4.6	9.8	6.7	1.8	7.7	–	–	10.4	6.4	17.4
Sp	0.2	–	–	–	–	–	–	–	–	2.7
Gt	6.1	19.2	2.5	5.9	7.7	6.4	6.0	15.4	6.1	–
$Fe^{3+}/\Sigma Fe$										
Ol	–	–	–	–	–	–	–	–	–	–
Opx	0.06	0.07 *	0.07 *	0.07 *	0.08	0.05 *	0.05 *	0.07 *	0.07 *	0.05
Cpx	0.12	0.27	0.18	0.21	0.13	–	–	0.24	0.12	0.19
Sp	0.12 *	–	–	–	–	–	–	–	–	0.26
Gt	0.034	0.044	0.115	0.108	0.12	0.074	0.072	0.046	0.034	
WR	0.019	0.045	0.023	0.021	0.025	0.012	0.016	0.023	0.017	0.036
SiO_2	46.5	49.6	47.0	45.7	45.2	46.3	48.3	44.7	44.6	46.1
MgO	42.6	35.7	42.1	44.2	43.0	44.7	40.7	39.2	44.6	37.5
Fe_2O_3	0.14	0.31	0.21	0.17	0.21	0.09	0.16	0.21	0.14	0.30
ΣFeO	6.8	6.14	8.1	7.2	7.51	6.8	9.2	8.3	7.3	7.56
CaO	1.43	3.01	1.63	0.9	2.01	0.56	0.96	2.93	1.68	3.64
Al_2O_3	1.68	4.98	0.83	1.41	1.87	1.24	0.61	3.68	0.74	4.08
TiO_2	0.01	0.04	0.05	0.2	0.03	0.05	0.02	0.19	0.11	0.14
Na_2O	0.08	0.16	0.12	0.08	0.13	0.07	0.04	0.14	0.10	0.37
Cr_2O_3	0.37	0.59	0.26	0.44	0.41	0.42	0.24	0.34	0.38	0.39
Total	99.5	100.2	100.1	100.1	100.2	100.1	100.1	99.5	99.5	99.8

Modes and bulk compositions given in wt%. * Not all phases available for analysis, estimated value. WR = whole rock. nd = no Fe^{3+} detected by ^{57}Fe Mössbauer spectroscopy.

statistical quality. Because orthopyroxene can comprise a large part of the mode in the samples studied, any uncertainty in its $Fe^{3+}/\Sigma Fe$ ratio results in a corresponding uncertainty in the Fe_2O_3 content derived for a whole rock sample. This effect is largest for the low-temperature southern African peridotites rich in orthopyroxene (Table 1). Conservative uncertainties in whole rock Fe_2O_3, for a change in $Fe^{3+}/\Sigma Fe$ of 0.02–0.10 in orthopyroxenes from orthopyroxene-rich southern African samples are plotted as error bars in one panel of Fig. 3. This kind of uncertainty dominates the propagated uncertainties in modal analyses, but should not alter the trends evident in the whole rock Fe_2O_3 data. The $Fe^{3+}/\Sigma Fe$ ratios for the clinopyroxenes, garnets and spinels analyzed also have variable uncertainties (see Appendix), particularly at values below 0.05, but their contribution to the uncertainty in whole rock Fe_2O_3 is subordinated by the uncertainty in $Fe^{3+}/\Sigma Fe$ for orthopyroxene.

As observed by Luth et al. [4], garnets from the high-temperature peridotites consistently contain more $Fe^{3+}/\Sigma Fe$ than those from low-temperature peridotites. In contrast, clinopyroxenes from the high-temperature peridotites generally have lower $Fe^{3+}/\Sigma Fe$ than those in low-temperature peridotites (Table 2), indicative of a temperature-dependent partitioning of Fe^{3+} between garnet and clinopyroxene. Details of this partitioning are pursued in a related study and for the sake of brevity are not described here.

Although the $Fe^{3+}/\Sigma Fe$ ratios of clinopyroxene, spinel and garnet are far greater than those of orthopyroxene, these minerals are generally in lower modal abundance, and contribute less than half of the bulk Fe_2O_3 of typical garnet peridotite. For garnet peridotites with 40–42 wt% MgO [29], orthopyroxene contributes 40–60% of whole rock Fe_2O_3, while clinopyroxene and/or garnet and/or spinel contribute 20–30%.

The correlation of Fe_2O_3 in peridotites with

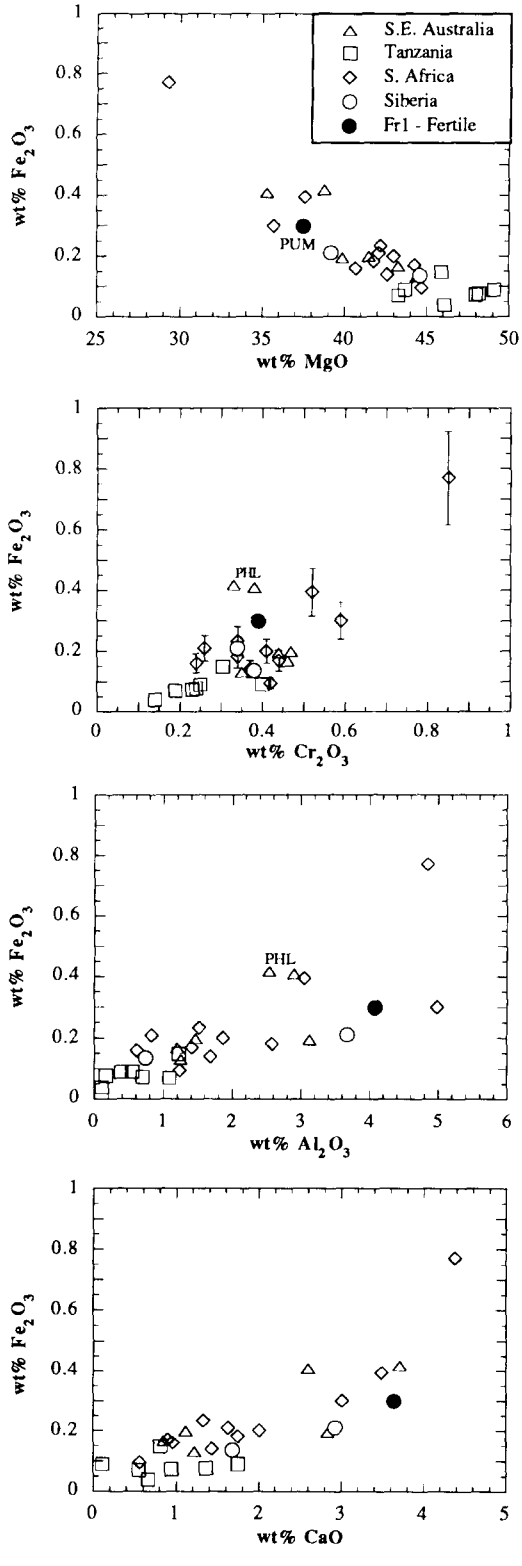

other elements can be used to derive the probable Fe_2O_3 contents and $Fe^{3+}/\Sigma Fe$ ratios for various mantle regions. For example, primitive upper mantle containing 37 ± 1 wt% MgO [15,29] is estimated to have a $Fe^{3+}/\Sigma Fe$ ratio of 0.036 (Fig. 2) or contain 0.3 wt% Fe_2O_3 (Fig. 3). These latter values, derived from trends in Figs. 2 and 3, are almost identical to the $Fe^{3+}/\Sigma Fe$ of 0.035 and 0.29 wt% Fe_2O_3 determined for a fertile peridotite, Fr1, with 37.64 wt% MgO (Table 2, Fig. 3). This latter sample was one of the primitive upper mantle candidates studied by Jagoutz et al. [15]. Average continental lithospheric mantle containing 40–45 wt% MgO would contain $\leqslant 0.2$ wt% Fe_2O_3. Very depleted peridotite from the ocean basins [30] or from trenches associated with subduction zones [31] would be most depleted in Fe_2O_3, with $\leqslant 0.1$ wt%. If cratonic mantle is considered to be as rich in orthopyroxene as average Kaapvaal mantle [17], it may represent a reservoir as rich in Fe_2O_3 as primitive upper mantle (Table 3).

Modally metasomatized xenoliths can contain large amounts of Fe_2O_3 bound in hydrous phases and represent some of the most Fe_2O_3-rich mantle (Fig. 3). These xenoliths may, in some cases, deviate away from the trends seen in the anhydrous samples and appear to have had Fe^{3+} added in the form of the metasomatically introduced hydrous phase [see also 26].

4. Oxygen buffers in the upper mantle

The Fe_2O_3 abundances determined for peridotites in this study now provide an opportunity for assessing the buffering capacity of all potential redox buffers in upper mantle assemblages

Fig. 3. Covariation in bulk Fe_2O_3 content of samples from this study with MgO, CaO Al_2O_3 and Fe_2O_3. Samples labelled PHL are two phlogopite-bearing southeastern Australian samples. Primitive upper mantle (PUM) with 37 wt% MgO [15,29] would contain ~0.3 wt% Fe_2O_3, identical to that determined for fertile sample Fr1. Error bars for the southern African samples in the Fe_2O_3 versus Cr_2O_3 diagram represent the uncertainty in calculated Fe_2O_3 for a change in the $Fe^{3+}/\Sigma Fe$ of orthopyroxene from 0.02 to 0.10.

and for understanding more clearly their potential role in controlling mantle oxidation states.

4.1. Iron

A plausible lower limit for the relative fO_2 in the Earth's mantle is FMQ − 4–FMQ − 5, which is the condition at which Fe–Ni metal will precipitate from typical upper mantle olivine containing 2500–3500 ppm Ni [32]. The $Fe^{3+}/\Sigma Fe$ of peridotite should be 0 at metal saturation, although a recent study has demonstrated that several high pressure mantle phases can have measurable $Fe^{3+}/\Sigma Fe$ ratios even at metal saturation [25]. At the higher fO_2 values recorded by anhydrous xenoliths in this study, the $Fe^{3+}/\Sigma Fe$ of peridotite varies in a non-systematic fashion (Fig. 4). A sporadic variation in Fe_2O_3 contents, from 0.1 to 0.4 wt%, is observed for most peridotites in this study over a range in fO_2 of FMQ − 3–FMQ + 3 (Tables 2 and 4). The estimated Fe_2O_3 content of 0.3 wt% for primitive upper mantle (Table 3, Fig. 3) represents a reservoir of 3×10^{22} mol O, or 6.6×10^{-6} mol O_2/g rock for the whole mantle. As will be shown below, this figure is comparable to the buffering capacity of any other oxygen buffer in the mantle.

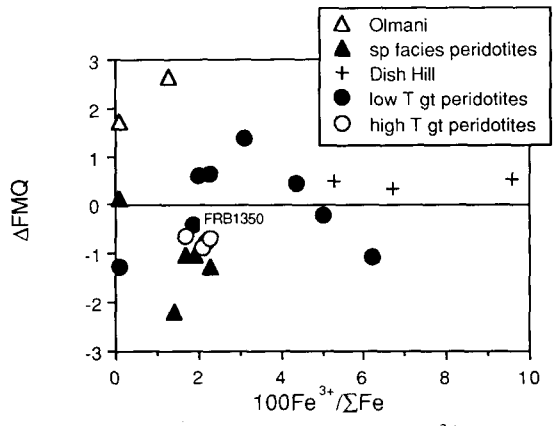

Fig. 4. Variation in the bulk percentage $Fe^{3+}/\Sigma Fe$ with $\log fO_2$ calculated relative to the FMQ buffer (ΔFMQ). Also shown are data for a metasomatized composite xenolith from Dish Hill [26]. ΔFMQ was calculated using ol–opx–sp equilibria for spinel-bearing assemblages and ol–opx–cpx equilibria for both spinel-free or garnet-bearing samples (Table 4). Note the extremely high fO_2 recorded by carbonatite-metasomatized samples from Olmani [8] and the similarity in fO_2 recorded by both high- and low-temperature garnet peridotites and by the graphite-bearing peridotite FRB1350.

Table 3
Mantle abundances and buffering capacities of Fe, C, H and S

	Fe_2O_3	C	C[a] (to buffer Fe)	S	S[a] (to buffer Fe)	H	H[a] (to buffer Fe)
Primitive[b] Mantle	0.3	80	75-150	200	40-80	245-290[g] 200-450[h]	225-450
MORB[c] Residue	~0.1	40	37	-	-	125-135[g] 10-130[h]	113
Cratonic[d] Mantle	~0.2	20[f]	75	-	-	176[g]	225
Subd.[e] Zone (Trench)	< 0.1	-	-	-	-	124[g]	<113

[a] The amount of C, H or S (in ppm) required to buffer Fe_2O_3 (in wt%) in a given mantle region according to reactions (1–3) in the text. Concentrations for Fe_2O_3 (in wt%) are estimated from Fig. 3 and those for C, S and H_2O are derived in the text. [b] From McDonough [29]. [c] From Dick and Fisher [30]. [d] From Boyd and Mertzman [17]. [e] From Bonatti and Michael [31]. [f] Average concentration in diamond-bearing samples [13,14]. [g] Calculated using maximum H_2O concentrations observed in mantle minerals. [h] Estimated from H_2O systematics in oceanic basalts.

4.2. Sulphur

The upper mantle probably contains 150–250 ppm S (or 6×10^{-6} mol/g), possibly existing as a sulphide liquid [36]. Near conditions of the NNO buffer this liquid may contain appreciable oxygen. For example, the O/(S + O) is about 0.5 in Fe–S–O liquids at the FMQ–FeS buffer [37]. Conversely, at metal saturation, sulphide liquids will have metal to sulphide ratios (M/S where M = Fe, Ni, Cu, etc.) greater than unity, the exact ratio depending on temperature and composition and on pressure, the effect of which is not well constrained. For an assumed M/S = 4, which represents metal saturation at 1200°C and 1 atm [38], the oxygen buffering capacity of the sulphide liquid hosting 200 ppm S in the mantle will be 1.2×10^{-5} mol/g, for changes in composition from $MS_{0.25}$ at metal saturation to $M(O_{0.5}S_{0.5})$ at the FMQ–FeS buffer. In this way, sulphide liquid in the whole mantle may represent an oxygen

reservoir of 5×10^{22} mol, perhaps even greater than Fe_2O_3.

4.3. Carbon

Published estimates for the C content of the mantle vary from 24 ppm [39] to 1000 ppm C [40], with direct measurements in mantle-derived xenoliths of 1–260 ppm, mainly as CO_2 in fluid inclusions [41] or as diamonds [13].

Estimates of C in more average portions of the mantle, such as the oceanic upper mantle, may be derived from the study of oceanic basalts. Blundy et al. [42] used a pre-degassing CO_2 content for MORB, estimated by Bottinga and Javoy [43], of 0.68 wt%, and suggested that MORB source mantle contains 680 ppm CO_2 (or 185 ppm C). The Bottinga and Javoy [43] initial MORB CO_2 content is 3–10 times higher than most measurements on quenched MORB glasses [44,45]. In contrast, Gerlach [46] used a mass balance of gas emissions to estimate that the initial CO_2 in transitional basalts from Afar was 0.12 wt% and suggested that this figure could be taken as an *upper limit* for the initial CO_2 content of MORB, as MORB is less enriched in incompatible elements. CO_2 contents of 0.32 and 0.65 wt% have been inferred for parental Kilauea magma by Greenland et al. [47] and Gerlach and Graeber [48], respectively. If Kilauea tholeiite represents 5% partial melting [49], then 40–90 ppm C may be present in the ocean island basalt source mantle.

A third potential estimate of mantle C can be derived from rare gas systematics. The ratio of $C/^3He$ in mantle gases is nearly constant [40] and this data, combined with the ^3He flux and basalt production at mid-ocean ridges, suggests mean MORB C contents of 400–600 ppm [50,51]. If average MORB is produced by 10% partial melting, then only 60–40 ppm C is required in the MORB source mantle, very near a recent estimate of 53 ppm for the degassed mantle, based on a more elaborate model for He and Ar systematics [52]. O'Nions and Oxburgh [51] also noted that C and K are correlated in major differentiation processes in the Earth, with an average K/C ratio of 3 on a weight basis. Thus, primitive mantle with approximately 240 ppm K [15,29] should contain about 80 ppm C.

The above evidence from rare gas systematics, and measurements of C in mantle peridotites and in MORBs, is most consistent with a C content in depleted MORB source mantle of about 40 ppm and about 80 ppm in the primitive upper mantle (Table 3). This corresponds to a reservoir of 7×10^{21} to 3×10^{22} mol O as CO_2 in the whole mantle, a value similar to, if not less than, that of Fe_2O_3. Nonetheless, it is clear from the divergent estimates reported above that any value from 1 to 250 ppm C could be adopted for the upper man-

Table 4
Oxygen fugacities and equilibration conditions of samples

Sample	T (°C)[a]	P (GPa)[b]	ΔFMQ ol-opx-sp[c]	ΔFMQ ol-opx-cpx[d]
Southeastern Australia				
84-402	998	1.5	-0.36	-1.03
85-168	1121	1.5	-0.56	-1.01
84-413	874	1.5	-	-1.42
BM134	908	1.5	-	-2.19
2905	963	1.5	-0.81	-1.24
Tanzania				
89-661	1090	4.5	-	0.13
89-680	1150	4.2	-0.05	0.60
89-719	1164	5.2	-	-1.27
89-777[e]	1120	2.0	1.71	-
89-773	1080	2.0	2.66	-
Southern Africa				
BD1140	975	5.0	-	-0.75
BD1150	1141	7.0	-	-0.20
BD1201	1007	6.3	-	1.37
BD1354	1294	9.0	-	-1.06
FRB1350[f]	722	2.5	-0.90	-0.42
FRB921	1055	4.2	-	0.43
FRB909	1395	6.2	-	-0.68
PHN5239	1431	7.1	-	-0.86
Siberia				
UV417/89	881	6.4	-	0.62
UV61/91	1239	7.8	-	-0.65

[a] Calculated using the two-pyroxene geothermometers of Wells [33] for sp + opx + cpx assemblages and Brey and Köhler [34] for gt + opx + cpx ± sp assemblages. [b] Assumed to be 1.5 GPa for sp + opx + cpx assemblages, except those from Olmani, which have an assumed pressure of 2.0 GPa [8]. Calculated for gt + opx + cpx ± sp assemblages using the method of Brey and Köhler [34]. [c] Calculated relative to the FMQ buffer using the method of Bryndzia and Wood [35]. Uncertainty ±0.7 log units. [d] Calculated relative to the FMQ buffer using the method of Luth and Canil [20] assuming ideal mixing on sites in clinopyroxene. Uncertainty ±0.7 log units. [e] ΔFMQ ol-opx-cpx cannot be calculated due to the lack of a $CaAl_2SiO_6$ component in clinopyroxene. [f] Fe^{3+} in spinel estimated from partitioning systematics between opx, cpx and sp.

tle and, therefore, the buffering capacity of C relative to Fe_2O_3 in the mantle remains highly uncertain.

4.4. Hydrogen

Hydrogen is considered here in a more convenient form as H_2O. Using direct measurements of H_2O concentrations in mantle minerals by infra-red spectroscopy, Bell and Rossman [53] estimate primitive upper mantle to contain 245–290 ppm H_2O in the garnet and spinel lherzolite facies, respectively (Table 3). Other, more depleted, mantle compositions, such as average abyssal peridotite [30] and average Kaapvaal mantle [17], contain 135 and 176 ppm H_2O, respectively, when the maximum H_2O contents of mantle minerals in Bell and Rossman [53] are used in the calculation (Table 3).

The H_2O content of the mantle can also be derived indirectly from H_2O concentrations in oceanic basalts. Byers et al. [54] predicted 200 ppm H_2O in the source region of the most primitive of the lavas they studied from the Galapagos Spreading Center. Based on H_2O and trace element systematics in MORB, Michael [55] estimated 100–130 ppm and 250–450 ppm H_2O in incompatible element depleted and enriched MORB source regions, respectively, and Dixon et al. [44] derived transitional and enriched MORB source abundances of 250 and 330 ppm, respectively. Dixon et al. [44] also produced an estimate of 10 ppm H_2O in MORB residues.

Using the H_2O systematics from oceanic basalts and maximum H_2O concentrations observed in mantle minerals, the primitive upper mantle probably contains between 250 and 450 ppm H_2O. These figures represent a reservoir of 5×10^{22} to 1×10^{23} mol O in the whole mantle; similar, if not larger, than those of Fe_2O_3 or C (Table 3).

4.5. Other elements

Of the other non-volatile elements in the mantle with variable valence states, only Cr and Ti have an abundance sufficient to influence $Fe^{3+}/\Sigma Fe$ ratios. Some Cr^{3+} may be reduced to Cr^{2+} even at terrestrial fO_2 values [56] but this would only be important at temperatures above 1500°C.

5. Controls on mantle oxidation states

The seemingly low oxygen buffering capacity of Fe^{3+}/Fe^{2+} equilibria in the volatile-free mantle has led to the contention that fO_2 in the upper mantle is more likely to be controlled by equilibria involving carbon [42,57]. Indeed, Blundy et al. [42] showed that the calculated fO_2 values of many spinel lherzolites fall within 1 $\log fO_2$ unit of the range calculated for carbon–carbonate equilibria at P–T conditions along likely geothermal gradients in the mantle.

Spinel peridotites from this study (Table 4) also have calculated fO_2 values that plot near the range calculated for carbon–carbonate equilibria by Blundy et al. [42]. However, the conclusion of Blundy et al. [46] regarding control of upper mantle oxidation states by carbon–fluid equilibria is questionable for two reasons. Firstly, as noted above, Blundy et al. [42] chose a rather high value for the C (or CO_2) content of the upper mantle, which is not supported by a number of other data. Secondly, their estimate of the Fe_2O_3 content and buffering capacity of Fe in peridotites only considered spinel and/or garnet as hosts for Fe^{3+}, but it is apparent that the contribution of pyroxenes to bulk Fe^{3+} is significant and essential for a more complete assessment of this parameter.

The crucial question is whether enough carbon exists in the mantle to buffer Fe^{3+}/Fe^{2+} equilibria, or vice versa. A mantle C abundance lower than the 185 ppm chosen by Blundy et al. [42] might indicate that it is only coincidental that the fO_2 recorded by Fe^{3+}/Fe^{2+} equilibria in mantle xenoliths is approximately similar to carbon–carbonate equilibria. For example, only 75 ppm C is required to reduce the 0.2 wt% Fe_2O_3 observed for the majority of peridotite residues in this study (Fig. 3) to FeO according to reaction (1). The re-appraisal of mantle C abundances given in Table 3 shows that the buffering capacities of C and Fe could be subequal in several regions of the mantle.

Primary, macrocrystalline, carbon (as either diamond or graphite) in mantle xenoliths is most often observed in samples representing cratonic mantle lithosphere [11,13,14]. Therefore, if any region of the mantle were to be buffered by carbon–carbonate equilibria, it would probably be beneath cratons. However, contrary to a recent proposal that the maximum fO_2 in the deep Archean lithosphere must be controlled by carbon–carbonate equilibria [57], the fO_2 values recorded by almost all cratonic garnet peridotites in this study are significantly above that of carbon–carbonate equilibria at the *P–T* conditions recorded by the samples (Fig. 5). Only sample FRB1350, a graphite-bearing peridotite from the Premier kimberlite in southern Africa, records an fO_2 near carbon–carbonate equilibria (Fig. 5). Thus, because carbon is inhomogeneously distributed in cratonic mantle lithosphere [11] it is likely to buffer fO_2 only locally. If carbon is also inhomogeneously distributed in both the continental and oceanic mantle lithosphere, then it is conceivable that the fO_2 values recorded by spinel lherzolite facies peridotites only fortuitously record fO_2 values coincident with carbon–carbonate equilibria and that both the garnet and spinel facies of the upper mantle are generally not buffered by carbon.

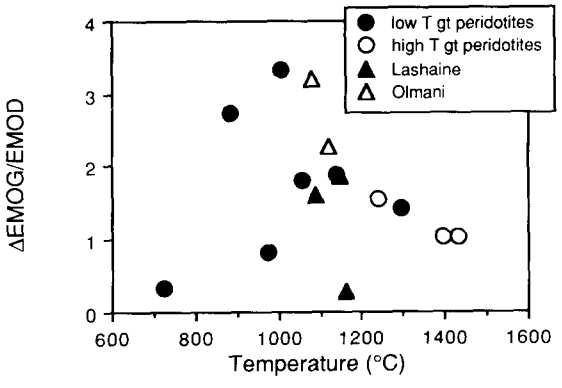

Fig. 5. Oxygen fugacities for garnet and spinel peridotite xenoliths from northern Tanzania, southern Africa and Siberia calculated relative to the carbon–carbonate buffers enstatite–magnesite–olivine–graphite (EMOG) and enstatite–magnesite–olivine–diamond (EMOD). The EMOG and EMOD buffers were calculated as in Eggler and Baker [58]. Circles and dots represent high- and low-temperature garnet peridotites, respectively, from both the Siberian and Kaapvaal cratons. Other samples as labelled. Note that most samples are far removed from the fO_2 of carbon–carbonate equilibria (EMOG/D) under these conditions.

The buffering capacity of H in the mantle appears, in many cases, to be larger than that of Fe_2O_3 (Table 3), but it is important to recognize that the mantle abundances deduced from basalt partial melting models for both H and C may be inflated values, if CO_2 and H_2O in the source region of basalts are concentrated from a larger volume of rock than the silicate melt [59]. It can be assumed that, within the uncertainty of the estimates, the buffering capacities of H and Fe_2O_3 are subequal for primitive upper mantle, MORB source, MORB residue and cratonic mantle. An exception may be mantle peridotite above subduction zones, which is likely to be depleted in Fe_2O_3 but rich in H, due to H_2O release from subducted oceanic lithosphere (Table 3). Evidence for enhanced H contents in the mantle source regions above subduction zones exists in the significant H_2O contents of magmas generated in this tectonic environment [60]. Subduction-related mantle is one example where the buffering capacity of H should be significantly above that of Fe_2O_3, perhaps explaining the highly oxidized arc-related magmas observed in nature [see also 57].

Sulphur is only likely to buffer mantle fO_2 if the S/O ratio in the mantle is sufficiently large [61]. However, the reservoir of S in the whole mantle is 5×10^{22} mol, roughly similar if not less than that of O, with 5×10^{22}–8×10^{22} mol. Unfortunately, little is known experimentally about the behaviour of sulphur during mantle melting, making it difficult to assess variations in its buffering capacity in the mantle.

Within the uncertainty in the mantle estimates for C, S and H, the capacities of Fe and these volatile elements to buffer oxygen in the upper mantle are all roughly equal. For this reason, the fO_2 and $Fe^{3+}/\Sigma Fe$ ratio of peridotite should, in most cases, be poorly buffered during melting and metasomatism in the upper mantle and no particular oxygen buffer system is expected to dominate the oxidation state of the upper mantle.

6. Ferric iron, oxygen fugacity and upper mantle processes

6.1. Melting

The Fe_2O_3 content of several residues in this study can be used to estimate the likely bulk distribution coefficient ($D^{Fe_2O_3}$) for Fe^{3+} during melting in the upper mantle. This is only an approximation, however, as $D^{Fe_2O_3}$ is likely to change with temperature, due to the temperature-dependent partitioning of Fe^{3+} between garnet and clinopyroxene noted above, and with pressure, due to the probable differences in $D^{Fe_2O_3}$ for spinel/melt and garnet/melt. The $D^{Fe_2O_3}$ during mantle melting can be estimated using the equation for batch melting:

$$C_l/C_o = 1/\left[\left(D^{Fe_2O_3} + f(1 - D^{Fe_2O_3})\right)\right] \quad (4)$$

where $D^{Fe_2O_3}$ = the bulk distribution coefficient for Fe_2O_3 between melt and peridotite residue; f = the degree of melting; and C_l and C_o = the concentrations of Fe_2O_3 in melt and residue, respectively. Using the average Fe_2O_3 content of 0.75 ± 17 wt% (1σ) for 78 MORB glasses [62], and assuming MORB is generated by 10% partial melting from a source peridotite with 0.1–0.2 wt% Fe_2O_3, results in a range of possible calculated values for $D^{Fe_2O_3} = 0.04$–0.2 using Eq. (4). However, almost the entire variation of $Fe^{3+}/\Sigma Fe$ ratios for peridotite residues shown in Fig. 2 can be explained by 5–40% batch melting of primitive upper mantle, assuming a constant $D^{Fe_2O_3}$ of 0.1. Use of the extreme values in $D^{Fe_2O_3}$ of 0.04 or 0.2 in the same calculations result in $Fe^{3+}/\Sigma Fe$ ratios for residues that are either too low, or too high, respectively, relative to those observed in the data set (Fig. 2). Thus, a constant $D^{Fe_2O_3}$ of ~ 0.1 seems a good approximation during mantle melting to explain the range of $Fe^{3+}/\Sigma Fe$ in the peridotite residues studied.

Assuming an upper limit for $D^{Fe_2O_3}$ of 0.2, Eq. (4) can be further applied to show that komatiites would have a maximum $Fe^{3+}/\Sigma Fe$ ratio of 0.08, if they are produced by more than 30% partial melting [63] from a primitive source mantle having a $Fe^{3+}/\Sigma Fe$ of 0.35 (Figs. 2 and 3). Using the method of Kress and Carmichael [64], this predicted upper limit of $Fe^{3+}/\Sigma Fe$ for typical Al-undepleted 'Munro type' komatiites (~ 25 wt% MgO) would correspond to an fO_2 of approximately NNO − 1.3 at a liquidus temperature of 1500°C. The latter estimated fO_2 value for komatiites is slightly above the average quenched in MORB glasses [62].

6.2. Metasomatism

Three samples in this study, from the Olmani cinder cone, Tanzania (Table 1), show evidence of metasomatism by carbonatite melt. This is shown by their extremely high Ca/Al ratios, low Al_2O_3 contents in clinopyroxene, extreme LREE enrichment, paucity of orthopyroxene, as well as the presence of monazite and apatite [8]. The relatively high fO_2 values calculated for two of the Olmani samples (Fig. 5, Table 4) are convincing evidence that metasomatism by carbonatite melts can have a significant effect on mantle oxidation states. This effect may have been magnified in the Olmani samples which, in order to explain their extreme degree of LREE enrichment, apparently underwent open system reaction with carbonatite and experienced metasomatism under high fluid/rock ratios [8]. Moreover, these samples are extremely depleted in Fe, making them more susceptible to changes in oxidation states produced by carbonatite metasomatism.

In contrast to the case of carbonatite metasomatism, other modally metasomatized and Fe_2O_3-rich samples from Dish Hill [26] and southeastern Australia (Table 1) record fO_2 values similar to that of average subcontinental mantle, with FMQ $\pm$ 1 (Fig. 4). No response of the fO_2 is, apparently, recorded by these and several other samples to modal metasomatism by hydrous silicate melt or fluid. The more observable effect of carbonatite metasomatism on mantle oxidation states (Fig. 6) relative to that of silicate melt/fluids may be due to the significantly larger O content available for reaction (and redox) in carbonatites compared to silicate melts. Alternatively, carbonate melts may simply be far more reactive than silicate melts during mantle–melt interaction.

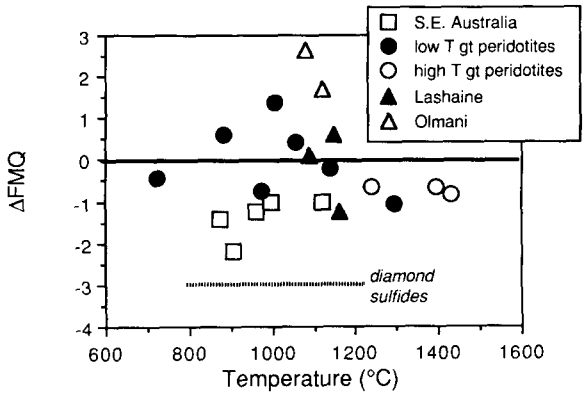

Fig. 6. Variation in logfO_2 relative to the FMQ buffer for all samples in this study calculated using ol–opx–sp equilibria for the Olmani samples and ol–opx–cpx equilibria for all others (Table 4). Circles and dots represent high- and low-temperature peridotites, respectively, from both Siberia and southern Africa. Also shown is the upper limit of fO_2 recorded by sulphide inclusions in diamonds [1].

The lack of any correlation between $Fe^{3+}/\Sigma Fe$ in peridotites with fO_2, or enrichment during metasomatism in samples from a broad range of tectonic environments, including cratons, is convincing evidence against any systematic 'buffering' of oxygen in any region of the upper mantle. Samples both with and without elemental carbon or hydrous phases (Table 1) all record similar fO_2 and have variable and uncorrelated $Fe^{3+}/\Sigma Fe$ ratios (Fig. 4). This observation is consistent with subequal buffering capacities for Fe, C, S and H in peridotites.

7. Spatial and secular variation in mantle oxidation state

Both secular and spatial variations in mantle oxidation state have a potential role in the evolution of the atmosphere [1] and have been the topic of several investigations [2,3,6,57]. The estimates presented for the oxidation state of garnet peridotites from cratonic mantle beneath southern Africa and Siberia in this study provide an opportunity for examining both spatial and secular variation in the oxidation states of ancient subcratonic mantle.

Cratonic mantle lithosphere may be unique in both composition and origin [17]. Isotopic studies of cratonic peridotites [12], the ages and equilibration temperatures of mineral inclusions in kimberlite-hosted diamonds from cratons [65,66] and geophysical considerations [67], require that cratonic mantle lithosphere was removed from the convective asthenosphere more than 3.0 Ga ago and stabilized to form 'keels', which extended to depths greater than 150 km. This part of the mantle has since experienced several enrichment or depletion events [12] but it is uncertain if such events have affected its oxidation state, or if the oxidation state of cratonic mantle differs from mantle lithosphere beneath orogenic belts or the ocean basins. Moreover, the oxidation state of cratons could give clues to the fO_2 attendant during diamond formation in this part of the mantle.

Cratonic peridotites record fO_2 values that scatter about the FMQ buffer (Figs. 4 and 6), well within the range observed for spinel lherzolite facies subcontinental mantle [2,3], but, in many cases, deviate well away from carbon–carbonate equilibria at similar pressures (Fig. 5). There is no apparent difference in the fO_2 recorded by low- and high-temperature garnet peridotites from the Kaapvaal craton (Figs. 4–6) or in the oxidation state of the mantle beneath the Kaapvaal craton between 1190 Ma, the age of eruption of kimberlite hosting the Premier samples, and 83 Ma, the eruption age of the Bultfontein samples (Tables 1 and 4). Considering the limited data available, there is also no distinct spatial variation in the oxidation state of cratonic mantle lithosphere beneath southern Africa and Siberia.

At assumed conditions of 1150°C and 5 GPa, the fO_2 values recorded by sulphide inclusions in diamonds from both the Siberian and Kaapvaal cratons cluster near FMQ − 3–FMQ − 4 [1]; significantly lower than that of cratonic garnet peridotites (Fig. 6). This may suggest that the oxidation states of both diamonds and their host cratonic lithosphere were similar, between FMQ − 3 and FMQ − 4, during the formation and stabilization of cratons, but that the lithosphere beneath these regions experienced oxidation, from which the sulphide inclusions were 'shielded' by their encapsulating diamond.

The oxidized nature of cratonic lithosphere relative to that predicted for the transition region [25] may provide an explanation for the origin of some diamonds and graphite in cratons. If kimberlite and other deep-seated intraplate magmas originate in the transition region [68], they may transfer reduced material to shallower levels for interaction with the deeper 'roots' of cratonic mantle lithosphere, producing reactions such as:

$$\underset{\text{fluid}}{CH_4} + 2\,\underset{\text{silicate}}{Fe_2O_3} = 2\,\underset{\text{melt}}{H_2O} + \underset{\text{diamond}}{C} + 4\,\underset{\text{silicate}}{FeO} \quad (5)$$

which result in graphite or diamond precipitation.

8. Conclusions

The Fe_2O_3 content of 28 bulk rock pyroxenite and peridotite samples is found to vary between 0.1 and 0.4 wt% Fe_2O_3. Primitive mantle probably contains 0.3 wt% Fe_2O_3 and has a $Fe^{3+}/\Sigma Fe$ ratio of 0.036.

Estimates of the bulk Fe_2O_3 content of peridotites from various regions in the upper mantle, when coupled with a re-assessment of the mantle abundances of C, S and H, indicate that the oxygen buffering capacities of Fe, S, C and H are subequal in most parts of the upper mantle. For this reason, oxygen fugacities in peridotite compositions are not likely to be controlled by any particular buffer system. This prediction is confirmed by the lack of any systematic correlation between $Fe^{3+}/\Sigma Fe$ with fO_2, or of fO_2 with the degree of depletion or enrichment observed in several samples [see also 3].

Oxygen fugacities calculated for garnet peridotites from northern Tanzania, Siberia and southern Africa are all within FMQ $\pm$ 1. The data show no evidence for: (1) systematic buffering of cratonic mantle lithosphere by carbon–carbonate equilibria; (2) any spatial variation in the oxidation state of lithosphere beneath cratons; or (3) any secular variation in the oxidation states of mantle lithosphere beneath the Kaapvaal craton in southern Africa between 1190 and 83 Ma. Cratonic mantle lithosphere is more oxidized than sulphide inclusions in diamonds, requiring progressive oxidation of the mantle beneath cratons since its formation and stabilization in the early Archean.

Acknowledgements

The authors are grateful to F.R. Boyd, H. Palme, N. Pokhilenko and P.H. Nixon for access to their xenolith collections, and to A. Woodland, B.J. Wood, F.R. Boyd and D. Ionov for reviewing the manuscript. G. Brey provided algorithms of his geothermobarometers and F.R. Boyd and H. Palme made available chemical data necessary for some of the modal calculations.

Appendix

Mineral separates (if available) for all phases from each sample were obtained by magnetic separation or heavy liquid techniques, followed by washing in dilute HCl or HF. The final separates used for ^{57}Fe Mössbauer spectroscopy were hand picked free of all visible alteration (i.e. to greater than 99% purity) under a binocular microscope. The amount of mineral separate produced after this process varied due to the amount of sample available. Mineral separates were not available for orthopyroxene in some of the samples studied (Table 2), but its $Fe^{3+}/\Sigma Fe$ ratio could be estimated using partitioning systematics (described in a companion study) for Fe^{3+} between orthopyroxene, clinopyroxene, spinel and garnet in the other xenoliths from Table 1.

Transmission ^{57}Fe Mössbauer spectra for each mineral were recorded at room temperature on a triangular velocity, constant acceleration spectrometer with a $\sim$ 50 mCi ^{57}Co in Rh source. Because the recoil-free fractions of Fe^{2+} and Fe^{3+} at different sites (and therefore $Fe^{3+}/\Sigma Fe$) of the garnet structure may vary as a function of temperature [19], Mössbauer spectra for garnet samples were also measured at 80 K using a variable temperature cryostat. Mirror-image spectra were recorded over 512 channels with a velocity range of $\pm$5 mm/sec and calibrated using Fe metal foil at room temperature. The spectra were fit using PC-MOS software (CMTE Elektronik, D-85521 Riemerling, FRG) which folds the mirror-image spectra and fits the resultant resonant absorption envelope. Sample powders were sandwiched between two sheets of Fe-free Al foil or held in Teflon discs. Phlogopite samples were mixed with sugar to minimize preferred orientation effects.

Absorber concentrations varied between 2 and 5 mg Fe/cm^2, depending on the amount of sample separated. Luth and Canil [20] showed that $Fe^{3+}/\Sigma Fe$ ratios derived for pyroxenes are insensitive to absorber concentrations within this

range. The $Fe^{3+}/\Sigma Fe$ ratio determined at 298 K for the PHN5267 garnet in this study was also measured as a function of absorber thickness and found to be constant over the range 2–5 mg Fe/cm^2. No attempt was made to extrapolate or correct the resultant $Fe^{3+}/\Sigma Fe$ determined for the garnets at 80 K to lower temperatures.

^{57}Fe Mössbauer spectra for olivines were fit with two symmetric, quadruple split doublets for Fe^{2+}. No Fe^{3+} was detected in spectra for olivines. Orthopyroxene spectra were fit with three symmetric, quadruple split doublets for Fe^{2+} and one symmetric, quadruple split doublet for Fe^{3+}. Clinopyroxene spectra were fit as in Luth and Canil [20] and spinel and garnet spectra were fit as in Wood and Virgo [21] and Luth et al. [4], respectively. Extended discussions of the accuracy, validity and sensitivity of the $Fe^{3+}/\Sigma Fe$ determined for pyroxenes, garnets and spinels to different fitting procedures are given in those publications. Spectra for amphibole and phlogopite were fit with two symmetric, quadrupole split doublets for Fe^{2+} and one symmetric, quadrupole split doublet for Fe^{3+}. More elaborate fitting procedures have been used in the literature for both of these minerals [22], but changes in the fitting model adopted here did not alter the resultant $Fe^{3+}/\Sigma Fe$ ratio derived from the Mössbauer spectra, which is the primary concern in this investigation. An appendix of analytical data and ^{57}Fe hyperfine parameters for all samples is available upon request from D. Canil.

References

[1] J.F. Kasting, D.H. Eggler and S.P. Raeburn, Mantle redox evolution and the oxidation state of the Archean atmosphere, J. Geol. 101, 245–257, 1993.

[2] A.B. Woodland, J. Kornprobst and B.J. Wood, Oxygen thermobarometry of lherzolite massifs, J. Petrol. 33, 203–230, 1992.

[3] D.A. Ionov and B.J. Wood, The oxidation state of subcontinental mantle: oxygen thermobarometry of mantle xenoliths from central Asia, Contrib. Mineral. Petrol. 111, 179–193, 1992.

[4] R.W. Luth, D. Virgo, F.R. Boyd and B.J. Wood, Ferric iron in mantle derived garnets: implications for thermobarometry and for the oxidation state of the mantle, Contrib. Mineral. Petrol. 104, 56–72, 1990.

[5] D.H. Eggler, Upper mantle oxidation state: evidence from olivine–orthopyroxene–ilmenite assemblages, Geophys. Res. Lett. 10, 365–368, 1983.

[6] S.E. Haggerty and L.A.Tompkins, Redox state of the Earth's upper mantle from kimberlitic ilmenites, Nature 303, 295–300, 1983.

[7] W.F. McDonough and M.T. McCulloch, The southeast Australian lithospheric mantle: isotopic and geochemical constraints on its growth and evolution, Earth Planet. Sci. Lett. 86, 327–340, 1987.

[8] R.J. Rudnick, W.F. McDonough and B.W. Chappell, Carbonatite metasomatism in the northern Tanzanian mantle: petrographic and geochemical characteristics, Earth Planet. Sci. Lett. 114, 463–475, 1993.

[9] R.J. Rudnick, W.F. McDonough and A. Orpin, Northern Tanzanian peridotite xenoliths: a comparison with Kaapvaal peridotites and inferences on metasomatic interactions, in: Kimberlites, Related Rocks and Mantle Xenoliths, Vol. I (proceedings of the 5th Int. Kimberlite Conf.) H.O.A. Meyer and O. Leonardos, eds., pp. 336–353, 1992.

[10] D.A. Carswell and J.B. Dawson, Garnet peridotite xenoliths in South African kimberlite pipes and their petrogenesis, Contrib. Mineral. Petrol. 25, 163–184, 1970.

[11] D.G. Pearson, F.R. Boyd, S.E. Haggerty, J.D. Pasteris, S.W. Field, P.H. Nixon and N.P. Pokhilenko, The characterization and origin of graphite in cratonic lithospheric mantle: a petrological, carbon isotope and Raman spectroscopic study, Contrib. Mineral. Petrol., in press.

[12] R.J. Walker, R.W. Carlson, S.B. Shirey and F.R. Boyd, Os, Sr, Nd and Pb isotope systematics of southern African peridotite xenoliths: implications for the chemical evolution of subcontinental mantle, Geochim. Cosmochim. Acta 53, 1583–1595, 1989.

[13] K.S. Viljoen, P.M. Swash, M.L. Otter, D.J. Schulze and P.J. Lawless, Diamondiferous garnet harzburgites from the Finsch kimberlite, North Cape, South Africa, Contrib. Mineral. Petrol. 110, 133–138, 1992.

[14] S.R. Shee, J.J. Gurney and D.N. Robinson, Two diamond-bearing peridotite xenoliths from the Finsch kimberlite, South Africa, Contrib. Mineral. Petrol. 81, 79–87, 1982.

[15] E. Jagoutz, H. Palme, H. Baddenhausen, K. Blum, M. Cendales, G. Dreibus, B. Spettel, V. Lorenz and H. Wänke, The abundances of major, minor and trace elements in the earth's mantle as derived from primitive ultramafic nodules, Proc. Lunar Planet. Sci. Conf. 10th, 2031–2050, 1979.

[16] B. Harte, Rock nomenclature with particular relation to deformation and recrystallization textures in olivine-bearing xenoliths, J. Geol. 85, 279–288, 1977.

[17] F.R. Boyd and S.A. Mertzman, Composition and structure of the Kaapvaal lithosphere, South Africa, in: Magmatic Processes: Physicochemical Principles, B.O. Mysen, ed., pp. 13–24, 1987.

[18] H.L. Allsopp, J.W. Bristow, C.B. Smith, R. Brown, A.J.W. Gleadow, J.D. Kramers and O.G. Garvie, A summary of radiometric dating methods applicable to kimberlites and related rocks, in: Kimberlites and Related Rocks: Their Composition, Occurence, Origin and Emplacement, J.L. Ross, ed., pp. 349–359, 1986.

[19] G. Amthauer, H. Annersten and S.S. Hafner, The Mössbauer spectrum of ^{57}Fe in silicate garnets, Z. Kristallogr. 143, 14–55, 1976.

[20] R.W. Luth and D. Canil, Ferric iron in mantle-derived pyroxenes and a new oxybarometer for the upper mantle, Contrib. Mineral. Petrol. 113, 236–248, 1993.

[21] B.J. Wood and D. Virgo, Upper mantle oxidation state: ferric iron contents of lherzolite spinels by ^{57}Fe Mössbauer spectroscopy and resultant oxygen fugacities, Geochim. Cosmochim. Acta 53, 1277–1291, 1989.

[22] F.C. Hawthorne, Mössbauer Spectroscopy, in: Spectro-

scopic Methods in Minerology and Geology, Rev. Mineral. 18, 255–341, 1988.
[23] A.J. Stolz and G.R. Davies, Chemical and isotopic evidence from spinel lherzolite xenoliths for episodic metasomatism of the upper mantle beneath southeastern Australia, in: Oceanic and Continental Lithosphere: Similarities and Differences, M.A. Menzies and K.G. Cox, eds., pp. 303–330, 1988.
[24] S. Press, G. Witt, H.A. Seck, D. Eonov and V.I. Kovalenko, Spinel peridotite xenoliths from the Tariat Depression, Mongolia II: geochemistry and Nd and Sr isotopic composition and their implications for the evolution of the subcontinental lithosphere, Geochim. Cosmochim. Acta 50, 2601–2614, 1986.
[25] H.St.C. O'Neill, D.C. Rubie, D. Canil, C.A. Geiger, C.R. Ross II, F. Seifert and A.B. Woodland, Ferric iron in the upper mantle and in transition zone assemblages: implications for relative oxygen fugacities in the mantle, in: Evolution of the Earth and Planets, Geophys. Monogr. 74, IUGG Vol. 14, pp. 73–88, 1993.
[26] A.V. McGuire, M.D. Dyar and J.E. Nielson, Metasomatic oxidation of upper mantle peridotite, Contrib. Mineral. Petrol. 109, 252–264, 1991.
[27] J.E. Banfield, M.D. Dyar, and A.V. McGuire, The defect microstructure of oxidized mantle olivine, EOS Trans. Am. Geophys. Union 72, 478, 1991.
[28] A. Nakamura and H. Schmalzried, On the stoichiometry and point defects of olivine, Phys. Chem. Minerals 10, 27–37, 1983.
[29] W.F. McDonough, Constraints on the composition of the continental lithospheric mantle, Earth Planet Sci. Lett., 101, 1–18, 1990.
[30] H.J.B. Dick and R.L. Fisher, Mineralogic studies of the residues of mantle melting: Abyssal and alpine-type peridotites, in: Kimberlites II: The mantle and Crust Relationships, Proc. 3rd Kimberlite Conf., J. Kornprobst, ed., pp. 295–308, 1984.
[31] E. Bonatti and P.J. Michael, Mantle peridotites from continental rifts to ocean basins to subduction zones, Earth Planet. Sci. Lett. 91, 297–311, 1989.
[32] H. O'Neill and V.J. Wall, The olivine–orthopyroxene–spinel oxygen geobarometer, the nickel precipitation curve, and the oxygen fugacity of the Earth's upper mantle, J. Petrol. 28, 1169–1191, 1987.
[33] P.R.A. Wells, Pyroxene thermometry in simple and complex systems, Contrib. Mineral. Petrol. 62, 129–139, 1977.
[34] G. Brey and T. Köhler, Geothermometry in four phase lherzolites II. New thermobarometers, and practical assessment of existing thermobarometers, J. Petrol. 31, 1353–1378, 1990.
[35] L.T. Bryndzia and B.J. Wood, Oxygen thermobarometry of abyssal spinel peridotites: the redox state and C–O–H volatile composition of the Earth's suboceanic upper mantle, Am. J. Sci. 290, 1093–1116, 1990.
[36] H. O'Neill, The origin of the Moon and early history of the earth — a chemical model. Part 2: The Earth, Geochim. Cosmochim. Acta 55, 1159–1172, 1991.
[37] C.D. Doyle and A.J. Naldrett, The oxygen content of sulfide magma and its effect on the partitioning of nickel between coexisting olivine and molten ores, Econ. Geol. 82, 208–211, 1987.
[38] K.C. Hsieh, R. Schmid and Y.A. Chang, The Fe–Ni–S system: I. A thermodynamic analysis of the phase equilibria and calculation of the phase diagram from 1173 to 1623 K, High Temp. Sci. 23, 39–52, 1987.
[39] H. Wänke, G. Dreibus and E. Jagoutz, Mantle chemistry and accretion history of the Earth, in: Archean Geochemistry, A. Kröner, ed., pp. 1–24, Springer, Berlin, 1984.
[40] B. Marty and A. Jambon, C/He^3 in volatile fluxes from the solid Earth. Implications for carbon geodynamics, Earth Planet. Sci. Lett. 83, 16–26, 1987.
[41] T. Trull, S. Nadeau, F. Pineau, M. Polve and M. Javoy, C–He systematics in hotspot xenoliths: implications for mantle carbon contents and carbon recycling, Earth Planet. Sci. Lett. 118, 43–64, 1993.
[42] J. Blundy, J. Brodholt and B.J. Wood, Carbon fluid equilibria and the oxidation state of the upper mantle, Nature 349, 321–324, 1991.
[43] Y. Bottinga and M. Javoy, Mid-ocean ridge basalt degassing: bubble nucleation, J. Geophys. Res. 95, 5125–5131, 1990.
[44] J.E. Dixon, E. Stolper and J.R. Delaney, Infrared spectroscopic measurements of CO_2 and H_2O in Juan de Fuca ridge basaltic glasses, Earth Planet. Sci. Lett. 90, 87–104, 1988.
[45] D.J. Des Marais, Carbon abundance measurements in oceanic basalts: the need for a consensus, Earth Planet. Sci. Lett. 79, 21–26, 1986.
[46] T.M. Gerlach, Degassing of carbon dioxide from basaltic magma at spreading centers: I. Afar transitional basalts, J. Volcanol. Geotherm. Res. 39, 21–219, 1989.
[47] L.P. Greenland, W.I. Rose and J.B. Stokes, An estimate of gas emissions and magmatic gas content of Kilauea volcano, Geochim. Cosmochim. Acta 49, 125–129, 1985.
[48] T.M. Gerlach and E. Graeber, Volatile budget for Kilauea volcano, Nature 313, 273–277, 1985.
[49] J.R. Budahn and R.A. Schmitt, Petrogenetic modeling of Hawaiian tholeiitic basalts: a geochemical approach, Geochim. Cosmochim. Acta 49, 67–89, 1985.
[50] M. Javoy, F. Pineau and H. Delorme, Carbon and nitrogen isotopes in the mantle, Chem. Geol. 57, 41–62, 1986.
[51] R.K. O'Nions and E.R. Oxburgh, Helium, volatile fluxes and the development of continental crust, Earth Planet. Sci. Lett. 90, 331–347, 1988.
[52] Y. Zhang and A. Zindler, Distribution and evolution of carbon and nitrogen in the Earth, Earth Planet. Sci. Lett. 117, 331–345, 1993.
[53] D.R. Bell and G.R. Rossman, Water in Earth's mantle: the role of nominally anhydrous minerals, Science 255, 1391–1397, 1992.
[54] C.D. Byers, D.M. Christie, D.M. Muenow and J.M. Sinton, Volatile contents and ferric–ferrous ratios of basalt, ferro-basalt, and andesite and rhyodacite glasses from

the Galapagos 95.5° W propogating rift, Geochim. Cosmochim. Acta 48, 2239–2245, 1984.

[55] P.J. Michael, The concentration, behaviour and storage of H_2O in the sub-oceanic upper mantle: Implications for mantle metasomatism, Geochim. Cosmochim. Acta 52, 555–566. 1988.

[56] J.P. Li, H.St.C. O'Neill and F. Seifert, Subsolidus phase relations in the system $MgO–SiO_2–Cr–O$ in equilibrium with metallic Cr, and their significance for the petrochemistry of chromium, J. Petrol., submitted.

[57] C. Ballhaus, Redox states of lithospheric and asthenospheric upper mantle, Contrib. Mineral. Petrol. 114, 331–348, 1993.

[58] D.H. Eggler and D.R. Baker, Reduced volatiles in the system C–O–H: Implications to mantle melting, fluid formation, and diamond genesis, in: High Pressure Research and Applications in Geophysics, M. Manghanni and S. Akimoto, eds., vol. 12, pp. 237–250, 1983.

[59] D. McKenzie and M.J. Bickle, The volume and composition of melt generated by extension of the lithosphere, J. Petrol. 29, 625–679, 1988.

[60] A.J. Crawford, T.J. Falloon and D.H. Green, Classification, petrogenesis and tectonic setting of boninites, in: Boninites and Related Rocks, A.J. Crawford, ed., pp. 2–49, Unwin Hyman, 1989.

[61] D.H. Eggler and J.P. Lorand, Mantle sulfide geobarometry, Geochim. Cosmochim. Acta 57, 2213–2222, 1993.

[62] D.M. Christie, I.S.E. Carmichael and C.H. Langmuir, Oxidation states of mid-ocean ridge basalt glasses, Earth Planet. Sci. Lett. 79, 397–411, 1986.

[63] N.T. Arndt and C.M. Lesher, Fractionation of REEs by olivine and the origin of Kambalda komatiites, Western Australia, Geochim. Cosmochim. Acta 56, 4191–4204, 1992.

[64] V.C. Kress and I.S.E. Carmichael, Stoichiometry of the iron-oxidation reaction in silicate melts, Am. Mineral. 73, 1267–1274, 1988.

[65] S.H. Richardson, J.J. Gurney, A.J. Erlank and J.W. Harris, Origin of diamonds in old enriched mantle, Nature 310, 198–202, 1985.

[66] F.R. Boyd, J.J. Gurney and S.H. Richardson, Evidence for a 150–200 km thick Archean lithosphere from diamond inclusion thermobarometry, Nature 315, 387–389, 1985.

[67] T.H. Jordan, Structure and formation of the continental tectosphere, J. Petrol. Spec. Lithosphere Issue, 11–37, 1988.

[68] A.E. Ringwood, S.E. Kesson, W.O. Hibberson and N. Ware, Origin of kimberlites and related magmas, Earth Planet. Sci. Lett. 113, 521–538, 1992.